Acta Crystallographica Section F
Structural Biology and Crystallization Communications
ISSN 1744-3091

Purification, crystallization and preliminary X-ray crystallographic analysis of Rab27a GTPase in complex with exophilin4/Slp2-a effector

Leonard M. G. Chavas,[a,b]* Kentaro Ihara,[b] Masato Kawasaki,[b] Ryuichi Kato,[b] Tetsuro Izumi[c] and Soichi Wakatsuki[b]

[a]Faculty of Life Sciences, The University of Manchester, Michael Smith Building, Oxford Road, Manchester, Lancashire M13 9PT, England, [b]Structural Biology Research Center, Photon Factory, Institute for Materials Structure Science, High Energy Accelerator Organization (KEK), Tsukuba, Ibaraki 305-0801, Japan, and [c]Department of Molecular Medicine, Institute for Molecular and Cellular Regulation, Gunma University, Maebashi 371-8512, Japan

Correspondence e-mail: leonard.chavas@manchester.ac.uk

Received 11 March 2008
Accepted 5 April 2008

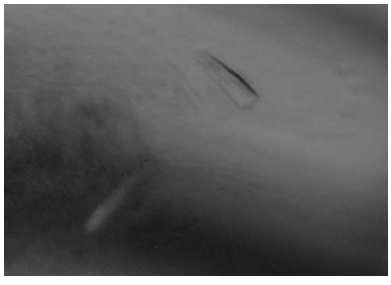

By switching between GTP-active and GDP-inactive conformations, small Ras GTPases partly regulate membrane trafficking, cell growth and cytoskeleton dynamics. Among Rab GTPases, the Rab27 subfamily, which comprises Rab27a and Rab27b, controls the proper targeting of secretory vesicles to the plasma membrane. GppNHp-bound Rab27a in complex with the Rab27-binding domain of exophilin4/Slp2-a effector has been purified and crystallized for structural studies. The crystals belong to space group $P2_12_12_1$ and a complete data set was collected to a resolution of 1.8 Å. Eventually, the structural characterization of the Rab27a–exophilin4/Slp2-a complex will clarify Rab27 recognition by its effectors prior to vesicle tethering and docking.

1. Introduction

Eukaryotic cell integrity strongly relies on membrane-trafficking events and their regulation. An estimated 60–100 different proteins belonging to independent subfamilies, such as Arf, Ras, Rho, Ran and Rab small GTPases, control a diverse array of signal transduction and intracellular transport events (Wennerberg *et al.*, 2005). More precisely, Arf and Arf-like proteins supervise different kinds of membrane fusion, including vesicle formation, secretion and endocytosis (Gillingham & Munro, 2007). Ras proteins are involved in a variety of intracellular signalling pathways that direct cell growth, differentiation and apoptosis in response to the activation of membrane-bound receptors (Omerovic *et al.*, 2007). The Rho-family proteins are required in cytoskeleton organization by controlling actin and microtubule dynamics, cell polarity and membrane transport, and play a role in release processes in granulocyte cells (Buchsbaum, 2007). Ran GTPases tune key events inside the eukaryotic nucleus such as nuclear transport, nuclear pore assembly, mitotic spindle assembly and DNA replication (Joseph, 2006). Finally, the members of the Rab/Ypt/Sec4 family act as essential regulators of vesicular transport (Grosshans *et al.*, 2006). Small GTPases adopt a G-domain fold, which consists of a mixed six-stranded β-sheet and five α-helices (Vetter & Wittinghofer, 2001). Two conserved regions called switch elements are directly associated with nucleotide binding. The switch elements are stabilized by GTP binding, while they adopt a relaxed conformation when bound to GDP (Dvorsky & Ahmadian, 2004).

The life cycle of Rab proteins is subject to strict synchronization, tightly coordinated by partner proteins such as guanine-dissociation inhibitors, GTPase-activating proteins or guanine-nucleotide exchange factors (Pfeffer, 2005). Localized on distinct vesicles and organelles, Rabs associate with downstream effector proteins in order to fulfill their role of vesicle transporter. This association is regulated spatially and temporally by their nucleotide state, where the hydrolysis of GTP to GDP turns off the Rab protein as a result of conformational rearrangements that disrupt the interaction with effectors (Kawasaki *et al.*, 2005; Pan *et al.*, 2006). The Rab27 subfamily, which consists of Rab27a and Rab27b, undertakes the transport of lysosome-related organelles or secretory lysosomes by recruiting disparate effector proteins in a cell-type specific manner (Izumi, 2007; Fukuda, 2006). Among 11 different Rab27 effectors,

exophilin4/Slp2-a bridges plasma-membrane phospholipids and Rab27 *via* interactions through C-terminal C2 domains and an N-terminal Rab27-binding domain, respectively, allowing peripheral localization of melanosome and glucagon granules (Kuroda & Fukuda, 2004; Yu *et al.*, 2007).

To date, numerous X-ray structures of Rabs alone or with partner proteins have been solved (for an overview, see Eathiraj *et al.*, 2005) and we have previously reported the crystal structure of GDP-bound Rab27b (Chavas *et al.*, 2007). However, additional insights are needed in order to fully unravel the differences existing among Rabs that lead to specific complex formation with their effectors, as mutations leading to functional impairment of Rab27a isoforms are illustrated by diseases such as Griscelli syndrome in humans, Hermansky–Pudlak syndrome or choroideremia (Seabra *et al.*, 2002). To obtain the structure of Rab27a in complex with exophilin4/Slp2-a will be a first step towards understanding its regulatory mechanism of vesicular transport at the molecular level.

2. Materials and methods

2.1. Cloning

To increase the probability of protein crystallization, the C-terminal hypervariable region of GTPase-inactive mouse Rab27a $_{r27}$Glu78Leu mutant was shortened by 18 residues during cloning; similarly, human exophilin4/Slp2-a was limited to its Rab27-binding domain. Thus, DNA segments coding for residues $_{r27}1$–$_{r27}193$ and $_{exo}10$–$_{exo}62$ (where the subscripts r27 and exo refer to Rab27 and exophilin4/Slp2-a, respectively) were amplified by polymerase chain reaction, cloned into the TOPO TA cloning vector (Invitrogen) and confirmed by nucleotide sequencing. Two cysteines in the Rab27 sequence might modulate effector recognition by forming an intramolecular disulfide bridge (Chavas *et al.*, 2007); therefore, two cysteine mutations $_{r27}$Cys123Ser and $_{r27}$Cys188Ser were additionally introduced following the QuikChange (Stratagene) procedure. After verifying the gene sequences, both constructs were subcloned into pGEX-4T-1 vector (Amersham Biosciences) and the plasmids were independently transformed into *Escherichia coli* strain BL21(DE3)-LysS.

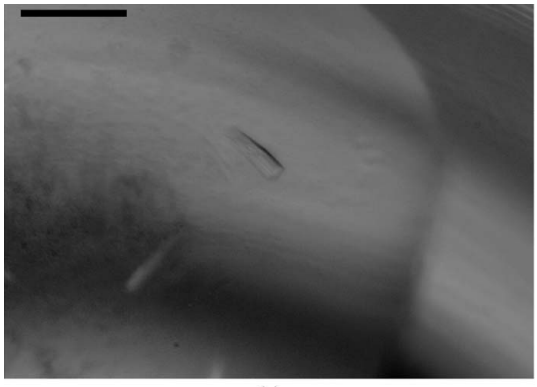

Figure 1
Crystals of Rab27a–exophilin4/Slp2-a. (*a*) Orthorhombic crystals obtained from a hanging drop. (*b*) A crystal in a cryoloop during data collection. The bars in the crystal pictures represent 0.2 mm.

2.2. Expression and purification

Rab27a $_{r27}1$–$_{r27}193$ bearing mutations $_{r27}$Glu78Leu, $_{r27}$Cys123Ser and $_{r27}$Cys188Ser and exophilin4/Slp2-a $_{exo}10$–$_{exo}62$ (referred to hereafter as Rab27a and exophilin4/Slp2-a, respectively) were separately overexpressed and purified. For expression of the recombinant proteins, one bacterial colony was used to inoculate 10 ml Luria–Bertani (LB) broth containing 50 µg ml^{-1} ampicillin, followed by overnight incubation at 310 K. The preculture was then transferred into 500 ml fresh LB medium supplemented with 50 µg ml^{-1} ampicillin and grown at 310 K for another 2 h. On reaching an OD_{660} of 0.6–0.8, cells were induced with 0.1 m*M* isopropyl β-D-1-thio-galactopyranoside and incubated for another 6 h at 303 K. The cells were finally harvested by centrifugation at 7000*g* for 15 min at 277 K. Cell pellets were resuspended in 30 ml lysis buffer (100 m*M* NaCl, 5 m*M* $MgCl_2$, 20 m*M* Tris pH 8.0) before being disrupted by sonication on ice.

Except where indicated otherwise, all purification steps were performed at 277 K. Soluble and membrane/insoluble fractions were separated by two rounds of centrifugation at 35 000*g* for 20 min; soluble samples were further filtered through an Ultrafree-MC 0.22 µm filter (Millipore) and incubated with 5 ml glutathione Sepharose 4B (GS4B) resin (Amersham Biosciences) for 4 h. In the case of Rab27a, the resin was loaded into a Poly Prep column (Bio-Rad) and washed with five volumes of EDTA buffer (lysis buffer containing 10 m*M* diaminoethanetetraacetic acid). Nucleotide exchange was then performed by equilibrating the resin with two volumes of GppNHp buffer {lysis buffer containing 1 m*M* guanosine 5′-[(β,γ)-imido]triphosphate}. The GST tag was cleaved on the resin by the addition of 5 units ml^{-1} thrombin protease (Amersham Biosciences) followed by 24 h incubation at 295 K. As a result of the cleavage by thrombin, two additional residues (Gly-Ser) are present in the N-terminal sequence of the Rab27a construct. The remaining protease and untagged Rab27a were eluted with 20 ml elution buffer [lysis buffer supplemented with 5 m*M* phenylmethylsulfonyl fluoride (PMSF) and 1 m*M* dithiothreitol (DTT)]. Complex formation with exophilin4/Slp2-a was performed on the effector-loaded GS4B resin by incubation with Rab27a for 2 h at 293 K. Uncomplexed proteins, inactivated thrombin and PMSF were removed by extensive washing with 20 volumes of lysis buffer. The Rab27a–exophilin4/Slp2-a complex was released from the resin by the addition of 5 units ml^{-1} thrombin followed by 12 h incubation at 295 K. Similarly to Rab27a, two residues are added to the exophilin4/Slp2-a N-terminal sequence after thrombin cleavage. Finally, the Rab27a–exophilin4/Slp2-a complex was eluted from the GS4B resin in elution buffer.

After concentration, impurities and thrombin were removed from the sample by size-exclusion chromatography purification through a Superdex-75 column pre-equilibrated with S75 buffer (150 m*M* NaCl, 1 m*M* $MgCl_2$, 20 m*M* Tris pH 8.0, 5 m*M* DTT) on an ÄKTA fast high-perfomance liquid-chromatography system (Amersham Biosciences). Fractions containing the pure complex were pooled and concentrated to 10 mg ml^{-1} using a Ultracel YM-10 Centricon filter (Millipore) (ε_{280} = 35 535 M^{-1} cm^{-1}) in S75 buffer, flash-frozen in liquid nitrogen and stored at 193 K. The purity of the samples was greater than 95% based on SDS–PAGE analysis.

Table 1
Crystal data and data-collection statistics for Rab27a–exophilin4/Slp2-a crystals.

Values in parentheses are for the highest resolution shell.

Space group	$P2_12_12_1$
Unit-cell parameters (Å)	a = 53.51, b = 77.78, c = 115.01
Matthews coefficient (Å^3 Da^{-1})	2.14
Solvent content (%)	42.5
No. of molecules per ASU	2
X-ray source	PF BL5A
Wavelength (Å)	1.0000
Resolution (Å)	30.3–1.8 (1.85–1.80)
Total observations	112804
Unique observations	45327
Completeness (%)	95.7 (98.6)
R_{merge} (%)	9.3 (63.4)
$\langle I/\sigma(I)\rangle$	6.5 (1.3)

2.3. Crystallization

Rab27a–exophilin4/Slp2-a complex crystals were grown at 289 K using the hanging-drop vapour-diffusion method. The volume of the drop was 2 µl, consisting of a mixture of 1 µl protein solution and 1 µl precipitant solution. The drop was equilibrated over a reservoir filled with 300 µl of a solution buffered at pH 6.5 and made up of 1.0 *M* sodium citrate trihydrate, 0.1 *M* sodium cacodylate. Orthorhombic crystals grew to maximum dimensions of 100 × 30 × 30 µm in 7 d (Fig. 1*a*).

2.4. X-ray data collection and processing

To carry out X-ray diffraction experiments, crystals were mounted in nylon loops (Hampton Research), flash-cooled in a 100 K dry nitrogen stream using reservoir solution supplemented with 20% ethylene glycol as a cryoprotectant and kept under the nitrogen stream during data collection. All diffraction data were indexed, integrated, scaled and merged using the *HKL*-2000 program suite (Otwinowski & Minor, 1997).

Beamline 5A at the Photon Factory (PF, Tsukuba) equipped with an ADSC Q315 CCD detector and a Rigaku cryosystem (X-Stream, Rigaku/MSC Inc.) was used to collect data from Rab27a–exophilin4/Slp2-a crystals. A single crystal of dimensions 90 × 30 × 20 µm (Fig. 1*b*) was exposed at an X-ray wavelength of 1.0000 Å and 62.5° of data were collected with 0.5° oscillation per image and an exposure time of 15 s at a crystal-to-detector distance of 213.1 mm.

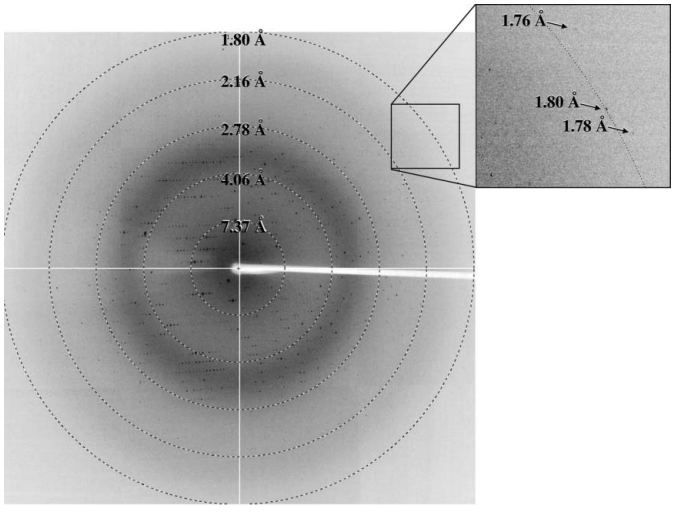

Figure 2
Diffraction pattern of Rab27a–exophilin4/Slp2-a crystals.

3. Results and discussion

In order to structurally characterize Rab27a–GppNHp in complex with exophilin4/Slp2-a, we independently cloned shortened constructs of both proteins ($_{r27}$1–$_{r27}$193 and $_{exo}$10–$_{exo}$62) into the pGEX-4T-1 vector containing an N-terminal GST tag followed by a thrombin protease cleavage site. We then purified the samples in large amounts by GST affinity, complex formation through pull-down assays and subsequent size-exclusion chromatography. Under denaturing and reducing conditions, SDS–PAGE showed a 1:1 heterodimer with single bands at about 25 and 8 kDa for Rab27a and exophilin4/Slp2-a, respectively. Diffraction-quality protein crystals were grown by the hanging-drop vapour-diffusion method, although sitting-drop methods also gave reasonable sized crystals using similar conditions. Crystals appeared from a reservoir solution containing sodium citrate as a precipitant and belonged to space group $P2_12_12_1$, with unit-cell parameters a = 53.51, b = 77.78, c = 115.01 Å. SDS–PAGE analysis of the crystals confirmed that they contained both proteins. For a protein molecular weight of 28 kDa (22 kDa for Rab27a and 6 kDa for exophilin4/Slp2-a), a calculated Matthews coefficient V_M (Matthews, 1968) of 2.14 Å^3 Da^{-1} (solvent content 42.5%) suggests the presence of two heterodimeric complexes per asymmetric unit. A self-rotation peak at $\kappa = 180^\circ$ further supports the twofold NCS assignment (data not shown). A complete data set was collected at a resolution of 1.8 Å (Fig. 2). Statistics of data collection and processing are summarized in Table 1. Structure solution of the Rab27a–exophilin4/Slp2-a complex by molecular replacement using the Rab27b (PDB code 2if0; Chavas *et al.*, 2007) structure coordinates as a search model is currently under investigation (our unpublished data; PDB code 3bc1).

We wish to thank the staff of beamline BL5A for help and useful discussions during data collection. Part of this work was supported by a Grant-in-Aid for Scientific Research (16570104) and the Protein 3000 project of the Ministry of Education, Culture, Sports, Science and Technology of Japan.

References

Buchsbaum, R. J. (2007). *J. Cell Sci.* **120**, 1149–1152.
Chavas, L. M. G., Torii, S., Kamikubo, H., Kawasaki, M., Ihara, K., Kato, R., Kataoka, M., Izumi, T. & Wakatsuki, S. (2007). *Acta Cryst.* D**63**, 769–779.
Dvorsky, R. & Ahmadian, M. R. (2004). *EMBO Rep.* **5**, 1130–1136.
Eathiraj, S., Pan, X., Ritacco, C. & Lambright, D. G. (2005). *Nature (London)*, **436**, 415–419.
Fukuda, M. (2006). *Biochem. Soc. Trans.* **34**, 691–695.
Gillingham, A. K. & Munro, S. (2007). *Annu. Rev. Cell Dev. Biol.* **23**, 579–611.
Grosshans, B. L., Ortiz, D. & Novick, P. (2006). *Proc. Natl Acad. Sci. USA*, **103**, 11821–11827.
Izumi, T. (2007). *Endocr. J.* **54**, 649–657.
Joseph, J. (2006). *J. Cell Sci.* **119**, 3481–3484.
Kawasaki, M., Nakayama, K. & Wakatsuki, S. (2005). *Curr. Opin. Struct. Biol.* **15**, 681–689.
Kuroda, T. S. & Fukuda, M. (2004). *Nature Cell Biol.* **6**, 1195–1203.
Matthews, B. W. (1968). *J. Mol. Biol.* **33**, 491–497.
Omerovic, J., Laude, A. J. & Prior, I. A. (2007). *Cell. Mol. Life Sci.* **64**, 2575–2589.
Otwinowski, Z. & Minor, W. (1997). *Methods Enzymol.* **276**, 307–326.
Pan, X., Eathiraj, S., Munson, M. & Lambright, D. G. (2006). *Nature (London)*, **442**, 303–306.
Pfeffer, S. R. (2005). *J. Biol. Chem.* **280**, 15485–15488.
Seabra, M. C., Mules, E. H. & Hume, A. N. (2002). *Trends Mol. Med.* **8**, 23–30.
Vetter, I. R. & Wittinghofer, A. (2001). *Science*, **294**, 1299–1304.
Wennerberg, K., Rossman, K. L. & Der, C. J. (2005). *J. Cell. Sci.* **118**, 843–846.
Yu, M., Kasai, K., Nagashima, K., Torii, S., Yokota-Hashimoto, H., Okamoto, K., Takeuchi, T., Gomi, H. & Izumi, T. (2007). *Mol. Biol. Cell*, **18**, 688–696.